



ELSEVIER

Contents lists available at ScienceDirect

Journal of Magnetism and Magnetic Materials

journal homepage: www.elsevier.com/locate/jmmmLocal magnetic behavior across the first order phase transition in $\text{La}(\text{Fe}_{0.9}\text{Co}_{0.015}\text{Si}_{0.085})_{13}$ magneto caloric compoundC. Bennati^{a,b,*}, F. Laviano^a, G. Durin^b, E.S. Olivetti^b, V. Basso^b, G. Ghigo^a, M. Kuepferling^b^a Department of Applied Science and Technology, Politecnico di Torino, C.so Duca degli Abruzzi 24, 10129 Turin, Italy^b Istituto Nazionale di Ricerca Metrologica (INRIM), Strada delle Cacce 91, 10135 Turin, Italy

ARTICLE INFO

Article history:

Received 22 June 2015

Received in revised form

20 July 2015

Accepted 29 July 2015

Available online 30 July 2015

Keywords:

Magneto-caloric

Magneto-optics

Phase transition

Dynamics

Micro-structure

ABSTRACT

We visualize, with a magneto optical imaging technique with indicator film, the local magnetic response of the compound $\text{La}(\text{Fe}_{0.9}\text{Co}_{0.015}\text{Si}_{0.085})_{13}$ during its first order magneto structural transition. The technique allowed us by comparing the stray fields of the main magneto caloric phase and of secondary phases present in the sample to obtain the magnetic behavior of each phase above and below the Curie temperature with respect to the surrounds. Computing the change in the total magnetic flux, when the sample crosses the Curie point, both in cooling and heating, we are able to correlate the average thermal hysteresis of the transition with the local magnetic properties at single sites and analyze the influence of defects on the transition dynamics.

© 2015 Elsevier B.V. All rights reserved.

1. Introduction

In the framework of solid state refrigeration, the last 30 years have been dedicated to the study of magneto-caloric compounds [1]. The magneto-caloric effect (MCE) origins from the change in the entropy of a system when forced by a magnetic field; in isothermal conditions the entropy change (ΔS_{iso}) results in an exchange of heat of the material which can be used to increase/decrease the temperature of the system [2]. Magnetic materials which shows a large MCE can give rise to temperature gradients up to 7 K with a 2 Tesla magnetic field [3]. These large magneto caloric effects are possible when, under the effect of an external magnetic field, a material undergoes a phase transition which involves changes both in the intrinsic magnetic order and structure.

The sharp paramagnetic (PM)/ferromagnetic (FM) phase transition in $\text{La}(\text{FeSi})_{13}$ based compounds was recently investigated by several research groups [4,5] and large ΔS_{iso} with low magnetic/temperature hysteresis were reported. For this reason the compounds still attract attention towards their use as active refrigerators in magneto cooling cycles. Many studies on the structural, magnetic and electronic properties demonstrated the first order nature of the phase transitions [6,7] with concurrent sharp jumps in magnetization (from PM to FM) and large negative lattice expansion [5] at the Curie point. To make the compounds suitable

for applications, Fe atoms can be partially substituted by Co, to adjust the Curie point towards higher temperatures (ambient), producing however a weakening of the first order nature of the transition [8].

A first order transition is characterized by an intrinsic latent heat decoupled from the continuous variation in the specific heat of a material. Since irreversibility is the cause of thermal and magnetic hysteresis when cycling MCE samples across the Curie point, its origin can be investigated with dedicated calorimetry experiments. Many results directed on shape and critical sizes of the materials suggested the fundamental role of micro-structure [9] in the hysteresis determination. However, these measurements, which can characterize the MCE properties of a material, provide volume informations, thus they make hard to distinguish between multiple contributions coming from the micro-scale. On the other side, Magnetic Force Microscopy (MFM) [10] and scanning Hall probe imaging techniques [11] have been already applied for this purpose, showing that single sites behavior can be quite different from the volume response. For this purpose, in the present work, we explore the local magnetic response at the surface of the compound $\text{La}(\text{Fe}_{0.9}\text{Co}_{0.015}\text{Si}_{0.085})_{13}$ using a Magneto-Optic Imaging technique with Indicator Film (MOIF). As we already showed previously [12], the technique is able to dynamically follow the magnetic phase transition across an entire surface of a sample without loosing micro-scale resolution on single sites, thus can be used to clarify some aspect related to local properties of the compound. The paper is organized as follows. We first provide the necessary information to understand the MOIF technique and its

* Corresponding author at: Department of Applied Science and Technology, Politecnico di Torino, C.so Duca degli Abruzzi 24, 10129 Turin, Italy.

E-mail address: cecilia.bennati@polito.it (C. Bennati).

application to magnetic materials. In the section results we show the quantitative data collected for different temperatures across the transition and we discuss the magnetic properties of defects and of the main phase. Finally we provide an interpretation of different dynamics observed in the compound when crossing the T_c based on previous results.

2. Material and measurement method

Polycrystalline Co substituted $\text{La}(\text{Fe}_x\text{Co}_y\text{Si}_{1-x-y})_{13}$ with $x=0.9$ and low Co content of $y=0.015$ and $T_c = 200$ K was prepared by powder metallurgy at Vacuumschmelze GmbH and CoKG [8]. The elemental analysis was performed by energy dispersive X-ray spectroscopy in a Scanning Electron Microscope (SEM) on a polished surface of the sample. Fig. 1 shows a representative area of the sample and the distribution of the constituent elements based on their X-ray characteristic energies. Two secondary phases can be distinguished from the La–Fe–Co–Si matrix: α –Fe grains and a La–O-rich phase with bright contrast in backscattered electrons images [13] which might be also conducted to the (1:1:1) phase of peritectic reaction: α –Fe + $\text{LaFeSi} \rightarrow \text{La}(\text{Fe}, \text{Si})_{13}$ [14]. The carbon-enriched spots are likely associated with diamond debris and organic matter accumulation in the pores of the sample, resulting from the sample polishing process. The α -Fe grains and the pores have typical sizes which span from 5 to 30 μm .

For the MOIF measurements, we fixed the sample on the cold finger of a cryostat with a transparent window. The thermal contact was completed by silver paint between the bottom surface of the sample and a flat disc of thin aluminium positioned on the top of the cold finger. A cernox thermometer is inserted between the aluminium disc and the cold finger to control the temperature of the sample. The technique [15,16] permits to visualize the stray field distribution at the surface of a magnetized object and is based on the use of garnet indicator films [17], which are sensitive to the out of plane component of the magnetic induction above the sample surface and some μm below it. The indicator film is a single crystal of Bismuth–Lutetium substituted iron garnet (BIG), deposited by liquid phase epitaxy on an optical substrate (Gadolinium–Gallium garnet) and equipped with a thin mirror (Ag) to amplify the signal. The BIG (Verdet constant $V=30^\circ \text{kOe cm}^{-1}$) is placed on the polished surface of the sample. As the magnetization inside the garnet rotates due to the stray field produced by the

sample, the light polarization changes according to Faraday constant of BIG. Real time images can be recorded and can be calibrated for each temperature of the measurement, subtracting a reference background (external field $H_a = 0$), and taking into account the response of the garnet to H_a and the parameter of the experimental setup [15].

3. Experimental

3.1. Field sweeps at fixed temperature

We identify different phases by comparison of MOIF images at temperatures above and below T_c ; in Fig. 2, we show on the same scale, the optical image of the sample and the two magnetic contrasted MOIF images. The optical image (a) indicates the presence of material defects (e.g. cracks, holes, etc.) which mainly correspond to the darker spots in the MOIF (b) when the sample is in its ferromagnetic phase. In the PM phase, Fig. 3(c), these “magnetic holes” are not visible any more, while bright random spots origin from magnetic grains corresponding to the α -Fe phase identified with the SEM.

The analysis has been performed on sets of frames taken at fixed temperatures while sweeping the external magnetic field between -75 and 75 mT perpendicular to the sample surface (z -direction). The measured z -component induction's field is given by

$$\mu_0 H_{meas} = \mu_0 (H_a + H_d), \quad (1)$$

the last term representing the dipolar field of the sample. Since the BIG is situated on top of the sample, we obtain a measure of the z -component of the local stray field present above the surface, H_{meas} . This field is dependent on the z -component of the magnetization according to magneto-static equations. We collected and modelled the hysteresis loops at each pixel position across the sample surface. Based on phenomenological observation we used Eq. (2) to fit the loops. We thus extract two parameters: the first, proportional to the external field and the second one, b , proportional to the cube of the external applied field

$$H_{meas} - H_a \approx a \cdot H_a - b \cdot H_a^3 \quad (2)$$

The linear coefficient, a , is conductible to the internal magnetic response of the sample, while b is a non-linear correction factor. In

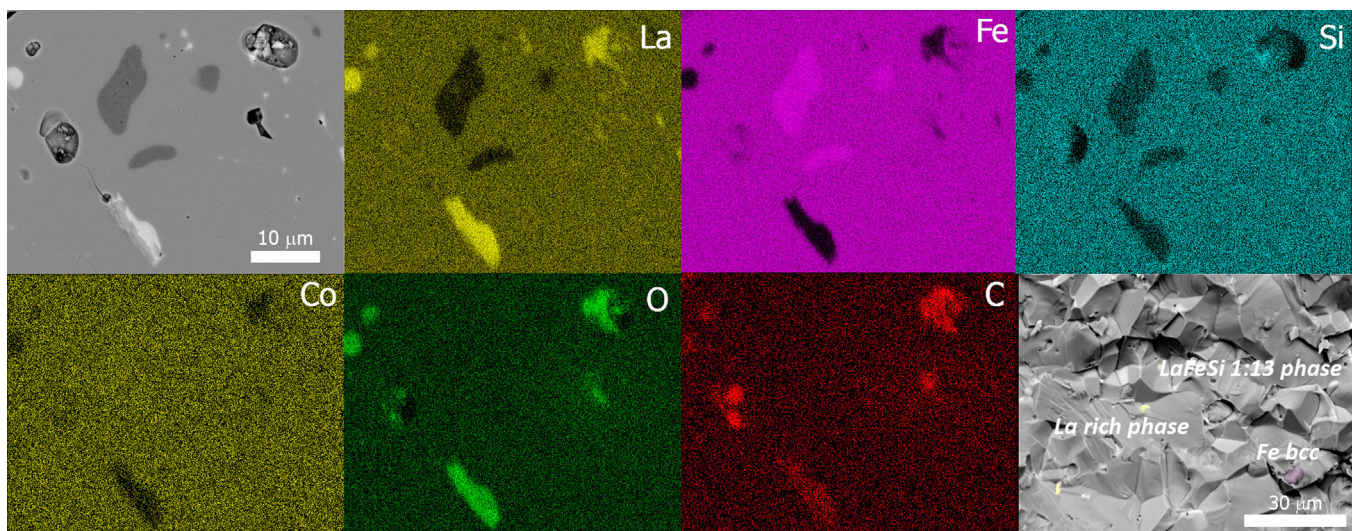


Fig. 1. SEM backscattered electrons image of sample surface and elemental X-ray maps of the area; the characteristic X-ray energies of selected elements (La, Fe, Si, Co, O, C) are represented in false colors. The bottom right image shows fracture surface of the sample where grains of the MCE phase are in grey and other phases are highlighted with the same colors of the X-ray maps. (For interpretation of the references to color in this figure caption, the reader is referred to the web version of this paper.)

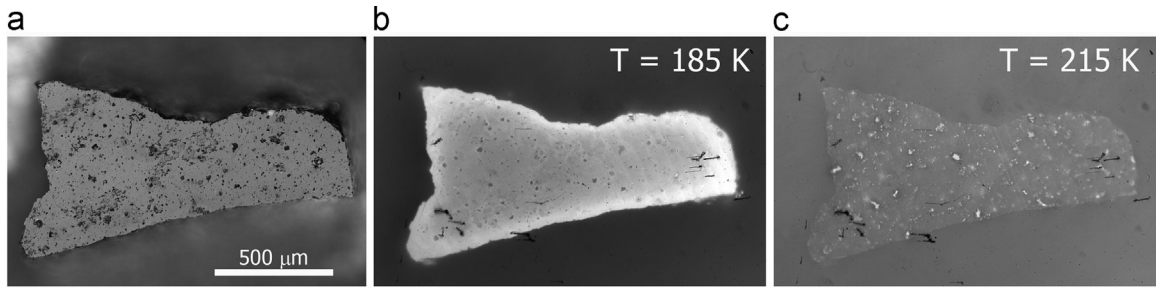


Fig. 2. (a) Optical image of the entire sample. MOIF images of the magnetic contrast in the ferromagnetic (b) and paramagnetic phase (c). The dark spots in the FM phase of the sample ($T=185$ K) mainly correspond to material defects in the optical image, while the bright spots in the PM phase (215 K) do not have a counterpart in the optical and FM images. In the MOIF images, the external magnetic field ($\mu_0 H_0 = 75$ mT) is pointing out of the images plane. MOIF images are raw data without calibration and are shown with different colour scales to highlight features coming from inhomogeneities.

Fig. 3(c) and (d) we show the maps of a for each pixel across the surface at temperatures above ($T=215$ K) and below T_c ($T=185$ K). These maps and their statistical distributions (**Fig. 3(a)** and (b)) permit to recognize two phases when $T > T_c$: the main MCE phase of the sample which behaves as a paramagnet with low $a=0.09$ and a second ferromagnetic phase of the α -Fe grains ($a=0.78$). When we performed the same local statistical analysis at $T < T_c$, we clearly see a drastic change of the a value of the MCE phase which overlaps with the value of the ferromagnetic grains, respectively, we found mean values of 1.54 and 1.37. Moreover, at this temperature, we found local minimum values of $a \approx 0.95$ randomly sparse at surface which represent the holes or local sites where the transition does not occur above 185 K.

In **Table 1** we summarize the values of a at $T=185$ K and 215 K

for the three different magnetic phases individuated: MCE main phase, α -Fe grains and magnetic holes.

The values of a have been calculated as the mean value of the statistical distributions of local pixels (grains). Both α -Fe and magnetic holes represent a fraction below the 2% of the total sample surface. As we already say, at $T=185$ K, the statistical distributions of the main MCE phase and α -Fe grains collapse to a similar value. This can be a confirmation of what was already observed in [10], where was found a peculiar behavior in the ferromagnetic X-ray magnetic dichroism signal of isolated ferromagnetic grains present at the surface, which disappears below the Curie temperature. Above T_c the α -Fe grains are ferromagnetic and their stray field is observed clearly. Below T_c the matrix also becomes ferromagnetic, and the flux of the α -Fe grains is closed in

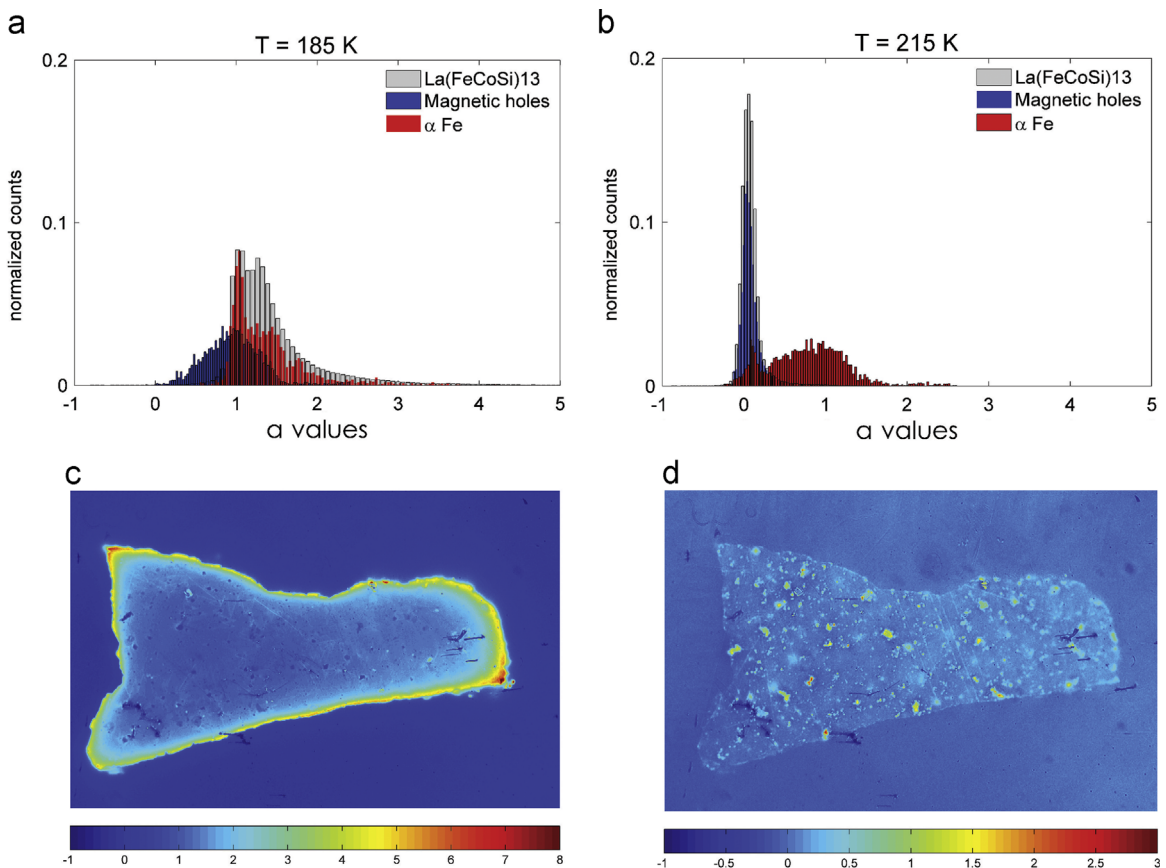


Fig. 3. (a) and (b) Statistics of the values of a at α -Fe and magnetic hole sites and of MCE phase below and above the Curie temperature and (c) and (d) respective local maps of the magnetic linear response across the sample. The values of counts have been normalized to make possible a comparison with the minor percentage of other phases (<2% of the total surface).

Table 1
Resume of the mean values of the linear coefficient a calculated for different phases and defects above (215 K) and below (185 K) the T_c .

| Phases | a | |
|----------------|-------|-------|
| | 185 K | 215 K |
| MCE phase | 1.54 | 0.09 |
| α -Fe | 1.37 | 0.78 |
| Magnetic holes | 0.95 | 0.10 |

the matrix, therefore it is not observable by MOIF.

Finally, from the statistical distributions in Fig. 3, we note that the magnetic holes individuated in the FM images have a large distribution of a when $T=185$ K, whether at the high temperature they behave as the rest of the PM phase. This is due to local stray fields of the ferromagnetic main MCE phase, which deviate due to the shape and magnetic irregularities produced by the magnetic holes at their surface.

3.2. Temperature sweeps at fixed field

Changing the temperature around the Curie point, we collected time/temperature sequences with resolution of ≈ 200 ms/ (11–15 mK/s) to map the discontinuous transition from the PM to the FM state (and vice versa) of the magneto-caloric phase. In these measurements, the external magnetic field was fixed at 30 mT perpendicular to the sample surface. We calculated from frames of the heating/cooling sequences the magnetic flux across the open top surface of the sample (at the distance of the garnet), by computing the integral of the product of z-component of stray field measured with the orthogonal surface of the sample.

Either in heating or in cooling, the growing of the new phase proceeds with some big jumps separated by almost continuous changes in the total magnetic flux. From Fig. 4 it is possible to recognize two big steps which correspond to two big parts of the sample transforming: looking at the pictures, the right side which transforms at lower T , and the left part which's T of transition is almost 0.5 K higher. The thermal hysteresis here reported was obtained from a correlation of the measured data by the frame rate and by removing an arbitrary offset to compare differences in the

PM/FM and FM/PM fronts advance. The dissimilarities in the thermal hysteresis of the two sides of the sample could be due to slight differences in composition (i.e. Curie temperatures) or due to slight differences in thermal contact between sample surface and the cold finger. However, thanks to the possibility to correlate the images of the whole surface with the total change in the magnetic flux, we notice, from some representative frames reported on the right of Fig. 4, that the two sides are not completely separated in temperature and some grains on the left start to transform with the big part on the right. Repeating the heating and cooling processes we observe that in both directions the nucleation of the new phase mainly starts from the edges of the sample and moves toward the center. The big pinning events which stop the phase front are almost the same in heating and cooling and seem to be related to mechanical stresses or cracks in the sample produced by the lattice expansion. At the end of the experiment, the sample was in fact divided in many pieces.

Due to the fact that the temperature at single local sites is not known, we cannot estimate quantitatively local hysteresis and correlate to the bulk one [18]. However, we qualitatively observe that, in spite of the slight faster temperature sweep rate, a longer time is spent in the linear part of the increasing total magnetic flux in cooling with respect to heating. In the heating process instead, we observe a re-entrance of the total magnetic flux just after the strong de-pinning of the left grains. To explain the slower cooling transition we individuated from MOIF frames a particular behavior of the FM front with respect to some α -Fe grains, around which, the FM transformation seems to be inhibited, an example is visible in Fig. 4 (frame h2) where an α -Fe grain in the middle of the sample is surrounded by the FM front. When the transition is completed and the magnetic flux is constant, as we pointed out in the previous section, the α -Fe grains disappear but magnetic holes in their vicinity are present.

Revisiting the previous results, some of the magnetic holes, which we have shown to possess a lower linear response with respect to the FM main phase, can be regarded as regions of the main phase with slightly different compositions, with a lower Curie temperature and a lower total magnetic moment. In our experiment, the magneto static field of magnetic phase front (FM) seems to interact with them and with α -Fe grains; beside the

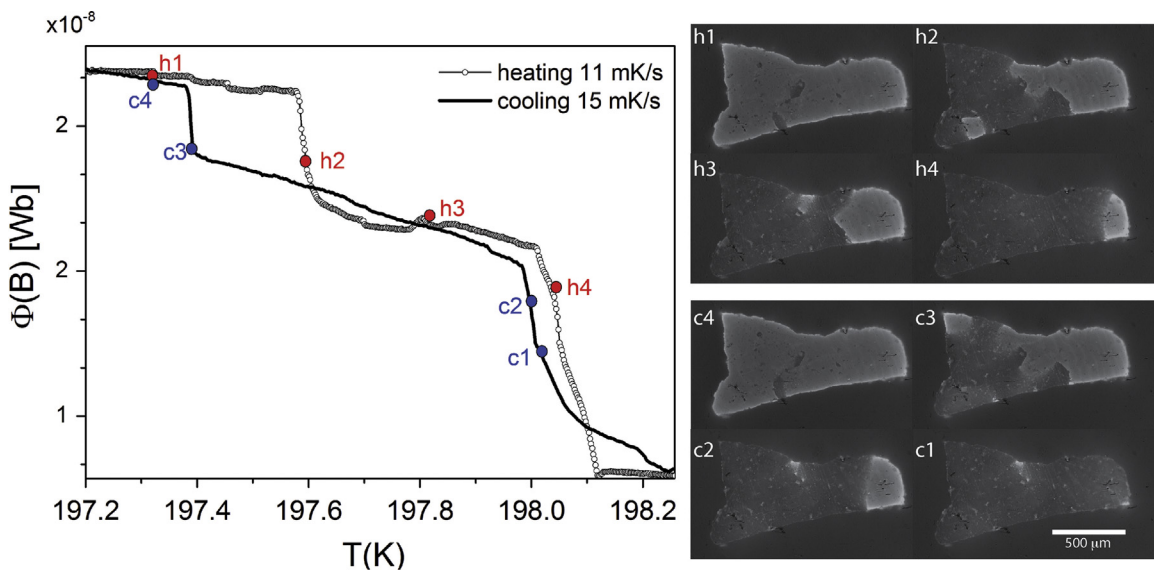


Fig. 4. Left graph: magnetic flux integrated across the surface of the sample during a heating (11 mK/s) and a cooling (15 mK/s) transitions. The graph was obtained by shifting the cooling curve in temperature by an arbitrary ΔT . The calibrated MOIF images on the right show the difference in the path followed by the surface ferromagnetic domains growth for the two temperature directions of the transition. In particular, h2 and c3, show that the energy barriers of bottom and up edges are very close to each other thus the one which disappear first is determinate by a random disordered process. An external biasing field of 30 mT is pointing out of the surface.

random nucleation process, the FM front advance seems to experience some magnetic friction.

4. Conclusions

The MOIF technique has been successfully applied to investigate the magnetic phase transition of the entire surface of $\approx 1000 \times 500 \mu\text{m}^2$ of a sample of the polycrystalline MCE compound $\text{La}(\text{Fe}_{0.9}\text{Co}_{0.015}\text{Si}_{0.085})_{13}$ above and below its Curie temperature ($\approx 198 \text{ K}$). The magnetic properties of the main MCE phase and of minor phases have been characterized and compared through the quantification of the local z-component of the stray field. Observing the phase transitions with temperature, we evaluate different sources of hysteresis individuating some of the extrinsic factors which introduce disorder. We observe how the low thermal hysteresis of this class of compounds can be affected differently by the type of defects, structural or magnetic, which modify differently the energy landscape of the PM/FM front.

The size and shape of the sample is crucial for our observation, structural defects or micro-cracks give rise to the big jumps, these effects can be overcome by optimizing synthesis processes and by reducing the dimension of the samples. On the other hand, the cooling nucleation process seems to be slowed down by the presence of magnetic impurities which introduce sources of random magnetic energy barriers and contribute to the hysteresis. To avoid extrinsic hysteresis sources in the design of MCE materials, a correct evaluation of defects due to grain boundaries has to be taken into account. The introduction of micro-sized defects of different magnetic nature, which is reported here as a source of hysteresis, can be explored towards an optimization of the functional properties of compounds. It may be helpful to explore the energy barriers created by magnetic impurities by changing external field and temperature sweep rate.

Acknowledgements

The research leading to these results has received funding from the European Union Seventh Framework Programme (FP7/2007–2013) under Grant agreement no. 310748.

References

- [1] K.A. Gschneidner, V.K. Pecharsky, Thirty years of near room temperature magnetic cooling: Where we are today and future prospects, *Int. J. Refrig.* 31 (2008) 945–961.
- [2] Aleksandr M. Tishin, Youry I. Spichkin, *The Magnetocaloric Effect and Its Applications*, IoP Publishing, Ltd., Bristol and Philadelphia (2003), p. 475.
- [3] E. Brück, O. Tegus, D.T. Thanh, H.H.J. Buschow, Magnetocaloric refrigeration near room temperature, *J. Magn. Magn. Mater.* 310 (2) (2007) 2793–2799.
- [4] S. Fujieda, A. Fujita, K. Fukamichi, Large magnetocaloric effect in $\text{La}(\text{Fe}_{1-x}\text{Si}_x)_{13}$ itinerant-electron metamagnetic compounds, *Appl. Phys. Lett.* 81 (2002) 1276–1278.
- [5] F.X. Hu, B.G. Shen, J.R. Sun, Z.H. Cheng, G.H. Rao, X.X. Zhang, Influence of negative lattice expansion and metamagnetic transition on magnetic entropy change in the compound $\text{LaFe}_{11.4}\text{Si}_{1.6}$, *Appl. Phys. Lett.* 78 (23) (2001) 3675–3677.
- [6] F.X. Hu, X.L. Qian, J.R. Sun, G.J. Wang, X.X. Zhang, Z.H. Cheng, B.G. Cheng, Magnetic entropy change and its temperature variation in compounds $\text{La}(\text{Fe}_{1-x}\text{Co}_x)_{11.2}\text{Si}_{1.8}$, *J. Appl. Phys.* 92 (7) (2002) 3620–3623.
- [7] A. Fujita, S. Fujieda, Y. Hasegawa, K. Fukamichi, Itinerant-electron metamagnetic transition and large magnetocaloric effects in $\text{La}(\text{Fe}_{1-x}\text{Si}_x)_{13}$ compounds and their hydrides, *Phys. Rev. B* 67 (10) (2003) 104416.
- [8] M. Katter, V. Zellmann, G.W. Reppel, K. Uestuener, Magnetocaloric properties of bulk material prepared by powder metallurgy, *IEEE Trans. Magn.* 44 (11) (2008) 3044–3047.
- [9] F.X. Hu, L. Chen, J. Wang, L.F. Bao, J.R. Sun, B.G. Shen, Particle size dependent hysteresis loss in $\text{La}_{0.7}\text{Ce}_{0.3}\text{Fe}_{11.6}\text{Si}_{1.4}\text{Co}_{0.2}$ first order systems, *Appl. Phys. Lett.* 100 (7) (2012) 072403.
- [10] V. Lollobrigida, V. Basso, F. Borgatti, P. Torelli, M. Kuepferling, M. Coisson, F. Offi, Chemical, electronic, and magnetic structure of LaFeCoSi alloy: surface and bulk properties, *J. Appl. Phys.* 115 (20) (2014) 203901.
- [11] K. Morrison, J.D. Moore, K.G. Sandeman, A.D. Caplin, L.F. Cohen, Capturing first- and second-order behaviour in magneto caloric $\text{CoMnSi}_{0.92}\text{Ge}_{0.08}$, *Phys. Rev. B* 79 (13) (2009) 134408.
- [12] M. Kuepferling, C. Bennati, F. Laviano, G. Ghigo, V. Basso, Dynamics of the magneto structural phase transition in $\text{La}(\text{Fe}_{0.9}\text{Co}_{0.015}\text{Si}_{0.085})_{13}$ observed by magneto-optical imaging, *J. Appl. Phys.* 115 (17) (2014) 17A925.
- [13] J. Liu, M. Krautz, K. Skokov, T.G. Woodcock, O. Gutfleisch, Systematic study of the microstructure, entropy change and adiabatic temperature change in optimized La-Fe-Si alloys, *Acta Mater.* 59 (9) (2011) 3602–3611.
- [14] X. Chen, Y. Chen, Y. Tang, High-temperature phase transition and magnetic property of $\text{LaFe}_{11.6}\text{Si}_{1.4}$ compound, *J. Alloys Compds.* 509 (34) (2011) 8534–8541.
- [15] F. Laviano, D. Botta, A. Chiodoni, R. Gerbaldo, G. Ghigo, L. Gozzelino, E. Mezzetti, An improved method for quantitative magneto-optical analysis of superconductors, *Superconduct. Sci. Technol.* 16 (1) (2003) 71.
- [16] F. Laviano, R. Gerbaldo, G. Ghigo, L. Gozzelino, G. Lopardo, B. Minetti, E. Mezzetti, Stacking procedure for noise reduction in magneto-optical imaging, *Phys. B: Condens. Matter* 403 (2) (2008) 293–296.
- [17] L.A. Dorosinskii, M.V. Indenbom, V.I. Nikitenko, Y.A. Ossip'yan, A.A. Polyanskii, V.K. Vlasko-Vlasov, Studies of HTSC crystal magnetization features using indicator magneto-optic films with in-plane anisotropy, *Phys. C: Superconduct.* 203 (1) (1992) 149–156.
- [18] M. Kuepferling, C.P. Sasso, V. Basso, Rate dependence of the magnetocaloric effect in La-Fe-Si compounds, *EPJ Web Conf. EDP Sci.* 40 (2013) 06010, p.